Molecular-weight dependence of morphology and mechanical properties of ultrahigh-molecular-weight polyethylene gel films

Tetsuya Ogita, Ryo Yamamoto, Nobuyasu Suzuki and Fumihiko Ozaki
Department of Polymer Materials Engineering, Faculty of Engineering, Yamagata University, Yonezawa 992, Japan

and Masaru Matsuo*
Department of Clothing Science, Faculty of Home Economics, Nara Women's University, Nara 630, Japan
(Received 2 February 1990; accepted 3 April 1990)

Films of three kinds of ultrahigh-molecular-weight polyethylenes (UHMWPE) with molecular weights of 6×10^6, 3×10^6 and 1×10^6 were produced by gelation/crystallization from dilute solutions. The dried gel films were stretched up to their maximum draw ratios. The molecular-weight dependences of morphology and mechanical properties of the drawn films have been examined using wide-angle X-ray diffraction, small-angle X-ray scattering, birefringence, crystallinity and stress relaxation modulus. It turned out that the long period, molecular orientation and crystallinity were hardly affected by molecular weight, while the stress relaxation modulus was strongly affected. The master curves indicated that the decrease in the stress relaxation modulus was more pronounced as the molecular weight of the test specimens decreased. This was thought to be due to a drastic increase of the slippage of molecular chains, leading to the disappearance of tie molecules and/or entanglement meshes under the external applied stress.

(Keywords: ultrahigh-molecular-weight polyethylene; gelation/crystallization; molecular-weight dependence; stress relaxation modulus; master curve)

INTRODUCTION

Gel deformation is well known as an excellent method to prepare high-modulus and high-strength polyethylene. This method was first proposed by Smith, Lemstra, Kalb and Pennings[1] and was mainly developed by Smith and Lemstra[2–4]. They demonstrated that the effective drawability of high-molecular-weight polyethylene made by the gel deformation method is dramatically enhanced using specimens spun or cast from semi-dilute solutions to form macroscopic gels. It turns out that, for a sufficiently high-molecular-weight polyethylene, the maximum achievable draw ratio depends principally on the concentration of solution from which the gel is made. This phenomenon is attributed to a reduced number of entanglements per molecule in solution-cast/spun polymers in comparison with those obtained from melts. The important problem is due to the fact that it was essentially impossible[5] to produce high-modulus and high-strength fibres (films) from gels using low-molecular-weight polyethylene (LMWPE) of molecular weight less than 3×10^5. Sawatari *et al.* have come to the conclusion that dry gels of LMWPE have very few entanglements that act as interlamellar crosslinks because of high crystallinity of the resultant dried gels. They pointed out that the length of total segments to form the amorphous phase within one polymer chain in the case of ultrahigh-molecular-weight polyethylene (UHMWPE) is much longer than that in the case of LMWPE. Namely, in the case of the same crystallinities, if the molecular weight of UHMWPE is 20 times larger than that of LMWPE, the total segments per molecule to form the amorphous phase for UHMWPE are almost 20 times longer than those of LMWPE.

Based on this concept, this paper deals with the molecular-weight dependence of morphological and mechanical properties of gel films in undrawn and drawn states using three kinds of polyethylenes with molecular weights of 6×10^6, 3×10^6 and 1×10^6 that form gel films. The specimens with different molecular weights were prepared by gelation/crystallization from solutions each with the most suitable concentration to ensure the maximum draw ratio. The morphological properties are mainly focused on the changes in crystallinity and molecular orientation with molecular weights at several draw ratios. The mechanical properties were discussed in terms of molecular-weight dependence of stress relaxation modulus. Actually, the temperature dependence of the stress relaxation modulus was measured in the range of time from 2 to 10^4 s and the master curve was constructed by shifting horizontally and then vertically. The activation energies obtained by the Arrhenius plots have been compared with those obtained by the dynamic measurements[6], since there has been no paper published on ultradrawn polyethylene in which the

* To whom correspondence should be addressed

0032-3861/91/050822-13

same value of activation energies concerning crystal dispersions has been obtained in comparison with the analysis obtained from master curves for the storage and loss moduli.

EXPERIMENTAL

The three kinds of linear polyethylenes used as specimens had viscosity-average molecular weights of 6×10^6 (Hercules 1900/90189), 3×10^6 (Hizex Million 240M) and 1×10^6 (Hizex Million 145M). For viscosity measurements, dissolution was carried out at 135°C under nitrogen and the solutions were stabilized with 0.1% w/w of antioxidant (di-t-butyl-*p*-cresol). The viscosities of the solutions were determined by an Ubbelohde-type capillary viscometer. Gels were prepared by crystallization from solution according to the method of Smith and Lemstra[2–4]. Decalin solutions containing approximate amounts of polyethylene and 0.1% of the antioxidant were prepared by heating the well blended polymer/solvent mixture at 135°C for 40 min under nitrogen. The homogenized solution was poured into an aluminium tray that was surrounded by ice–water to form a gel. The decalin was allowed to evaporate from the gels under ambient conditions for 30 days. The nearly dried gel was immersed in an excess of ethanol for several days and subsequently vacuum dried for 1 day to remove residual traces of the decalin–ethanol mixture. The resulting dry gel films were stretched in a hot oven at 135°C.

Density of the dry gel was measured by a pycnometer with chlorobenzene–toluene as a medium. Since the density is remarkably affected by the residual antioxidant, great care was taken to remove the antioxidant. The dry gel was cut into fragments and they were immersed in an excess of ethanol for several days and subsequently vacuum dried for 1 day prior to measuring the density.

The thermal behaviour was estimated in terms of melting endotherms of differential scanning calorimetry (d.s.c.) curves. Dry gels, weighing 3 mg, were placed in a standard aluminium sample pan. Samples were heated at a constant rate of 10°C min^{-1}.

Infra-red spectra were recorded by a Hitachi 285 in the range of bands from 1200 to 1400 cm^{-1}.

The X-ray measurements were carried out by 12 kW rotating-anode X-ray generator (Rigaku RDA-rA). Wide-angle X-ray diffraction (WAXD) and small-angle X-ray scattering (SAXS) patterns were obtained with a flat-film camera using Cu K_α radiation at 200 mA and 40 kV.

The second-order orientation factor F^j_{20} of the reciprocal lattice vector of the jth crystal plane is given by:

$$F^j_{20} = \int_0^{2\pi} \int_0^{\pi} \frac{1}{2}(3\cos^2\theta_j - 1) q_j(\cos\theta_j) \sin\theta_j \, d\theta_j \, d\phi_j \quad (1)$$

where θ_j and ϕ_j are the polar and azimuthal angles of the reciprocal lattice vector of the jth crystal plane with respect to the stretching direction, and $q_j(\cos\theta_j)$ is the orientation distribution function of the reciprocal lattice vectors of the jth crystal plane. The detailed experimental procedure was discussed elsewhere[7].

The stress relaxation modulus was measured for the period $2–10^4$ s over the temperature range 20–130°C using an auto-recording relaxometer, which was designed in our laboratory. The length of the specimen between the jaws was about 50 mm and the width was about 4 mm. During measurements, the films were subjected to a static tensile strain at 0.2% in order to place the sample in tension. A question arises whether the linearity of viscoelastic characteristics is valid. As an initial experiment, the linearity was confirmed from the recovery of strain at room temperature on the basis of detailed analysis of creep and recovery behaviour reported by Zapas and Crissman[8]. Before the measurements were made, the undrawn and drawn films were annealed for 1 h at 130°C under a fixed state.

RESULTS AND DISCUSSION

It has been found that, for a sufficiently high molecular weight, the maximum achievable draw ratio depends principally on the concentration of the solution. A question arises as to how an optimum concentration can be measured. Therefore, the gel films were prepared from solutions with different concentrations, in order to determine the optimum concentration to ensure maximum draw ratio. *Table 1* shows the concentration dependence of draw ratio and indicates the optimum concentrations to realize draw ratios up to draw ratio (λ) of 300 for three kinds of UHMWPE. The possibility of successful drawing up to $\lambda = 300$ becomes lower as the concentration moves away from each critical point. Accordingly, it may be expected that most of the chain molecules in the regime of low concentration are random coils having coupling entanglements that will be predominantly intramolecular in nature. On the other hand, solutions corresponding to the regime of high concentration are thought to consist of interpenetrating random coils, which form a large number of coupling entanglements that are both intra- and intermolecular. For specimens prepared from solutions with each critical concentration, it may be expected that there exists a suitable level of entanglement meshes that act as interlamellar crosslinks and effectively transmit the drawing force, and then the possibility that polymer chains wiggle through each other without interconnection is very small. As listed in *Table 1*, the critical point shifts to lower concentration with increasing molecular weight (MW). This is probably due to the fact that the number of coupling entanglement meshes of UHMWPE

Table 1 Concentration dependence of draw ratio for three kinds of dried gel films

Molecular weight, MW	Concentration (g/100 ml)	Achievable draw ratio, λ
1×10^6	1.2	300
	1.6	350
	2.0	250
	2.4	200
3×10^6	0.35	300
	0.5	350
	0.65	400
	0.8	300
	1.0	200
6×10^6	0.1	100
	0.2	200
	0.3	300
	0.4	400
	0.45	400
	0.5	300
	0.6	250

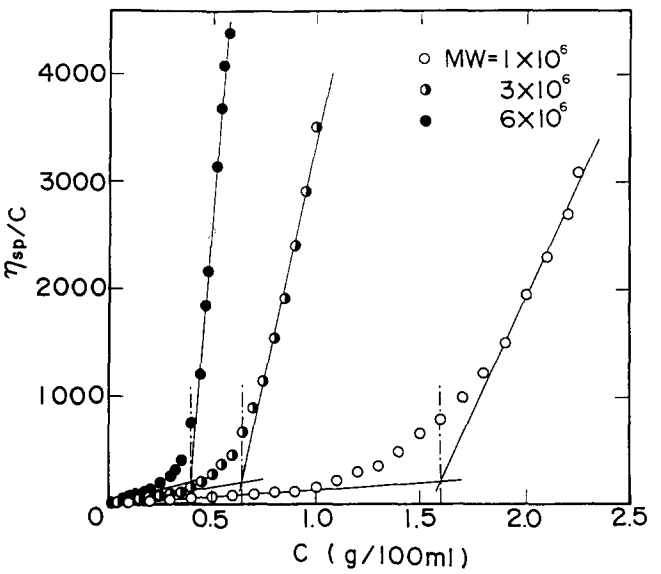

Figure 1 Relationship between reduced viscosity η_{sp}/c and concentration c for the solutions of three kinds of polyethylenes

with $MW = 6 \times 10^6$ increases drastically with increasing concentration.

In order to support this concept, measurements of solution viscosities were carried out, since viscosity is basically related to the size or extension in space of macromolecules. *Figure 1* shows the results, in which η_{sp} is defined by $\eta_{sp} = \eta/\eta_0 - 1$ using η and η_0 corresponding to the viscosities of solution and solvent, respectively. The data indicate that there exists a critical concentration range where there is an abrupt change in the concentration dependence of viscosity. Here it should be noted that the plots can be classified approximately into two reduced-viscosity regimes, one of low concentration dependence and the other of high concentration dependence. The two straight lines were drawn by a least-squares method, by which it was relatively simple to fit a tangent to the data. The intersection of the two lines shifts to lower concentration with increasing molecular weight. Interestingly, each intersection corresponds to each optimum concentration listed in *Table 1*.

Figure 2 shows the logarithmic plot of the optimum concentration (C_{opt}) and the reciprocal of the molecular weight ($1/MW$). The plot can be approximated as a straight line. If this is the case, this qualitative treatment led to the expectation that the optimum concentration can be derived as a function of molecular weight, but the analysis still remains an unresolved problem.

Figure 3 shows WAXD and SAXS patterns for the undrawn films prepared for each critical concentration, when an incident beam was directed parallel to the film surface (end view). The WAXD patterns for all the unannealed specimens indicate the preferential orientation of the c axis perpendicular to the film surface and the profile of the WAXD pattern is independent of the annealing effect. The SAXS patterns for unannealed specimens show scattering maxima in the meridional direction but the scattering maxima become indistinct for the specimens annealed at 130°C for 1 h. This means that there is an increase in orientational disorder and/or thickness fluctuations of the crystal lamellae that were oriented with their flat faces parallel to the film surface. Moreover, the scattering maxima move close to the centre of the pattern, which indicates an increase in long period. This behaviour is independent of the molecular weight and is similar to the annealing effect of single-crystal mats.

Table 2 presents crystallinity, long period and crystal lamellar thickness calculated from the values of long period for the unannealed specimens. The long period and the lamellar thickness become larger with increasing molecular weight, but within the experimental errors this tendency is not so significant. Incidentally, the increase in the long period is essentially independent of the concentration of solution used to prepare the gel films with $MW = 1 \times 10^6$ and 3×10^6. Such a phenomenon has been observed for the long period of a gel film with $MW = 6 \times 10^6$ prepared from solutions with concentrations in the range 0.1–0.6 g/100 ml[5].

Figure 4 shows the Young's modulus as a function of draw ratio for gel films with $MW = 1 \times 10^6$ prepared from solutions with 1.2 and 1.6 g/100 ml to ensure a draw ratio beyond 300. The Young's modulus of the specimen prepared with 1.6 g/100 ml is higher than that prepared with 1.2 g/100 ml. This behaviour is attributed to the difference in the number of entanglements per molecule. Judging from the results in *Figure 1*, it may be expected that the number of entanglements within the specimen prepared with 1.6 g/100 ml is more than in that prepared with 1.2 g/100 ml, and this relationship can be preserved even for the specimen drawn to $\lambda = 300$. The same tendency can be observed for the specimen with $MW = 3 \times 10^6$.

Through a series of experimental results, we used the samples from solutions with concentrations 0.4 g/100 ml for $MW = 6 \times 10^6$, 0.65 g/100 ml for $MW = 3 \times 10^6$ and 1.6 g/100 ml for $MW = 1 \times 10^6$ to ensure maximum drawability in the subsequent experiments.

Figure 5 shows the change in crystallinity with draw

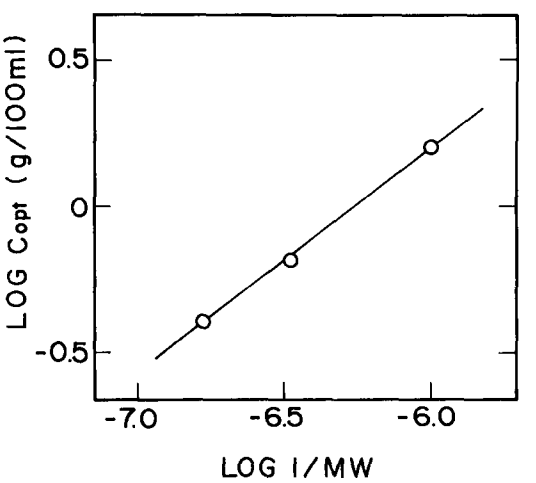

Figure 2 Logarithmic plot between the optimum concentration C_{opt} and the reciprocal of the molecular weight $1/MW$

Table 2 Crystallinity, long period and thickness of crystal lamellae for the dried gel films with the indicated molecular weight in an undeformed state

Molecular weight, MW	Crystallinity (%)	Long period (Å)	Thickness of crystal lamellae (Å)
1×10^6	84	110	92
3×10^6	83	114	95
6×10^6	83	119	99

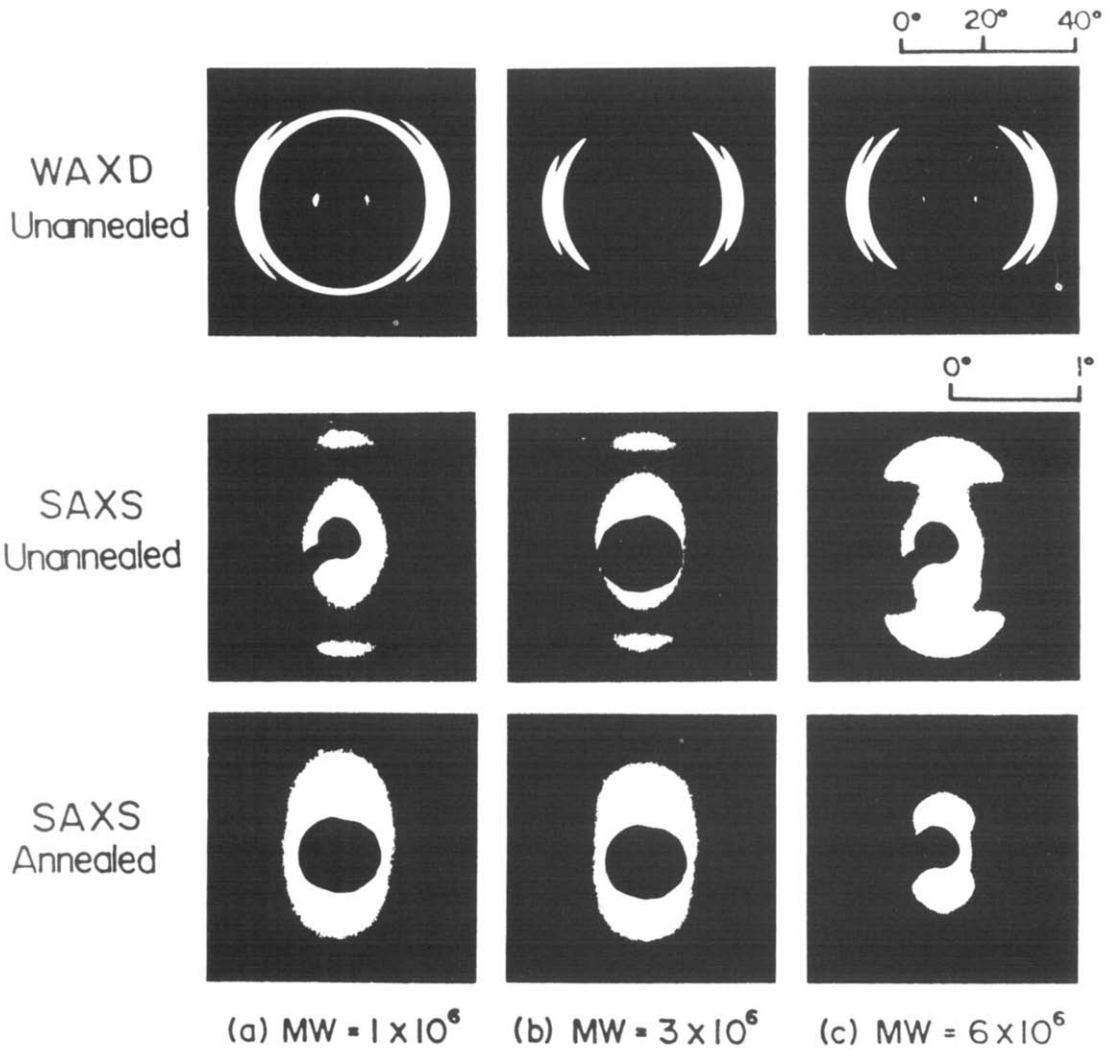

Figure 3 WAXD and SAXS patterns (end view) for the dried gel films with the indicated molecular weights in an undeformed state

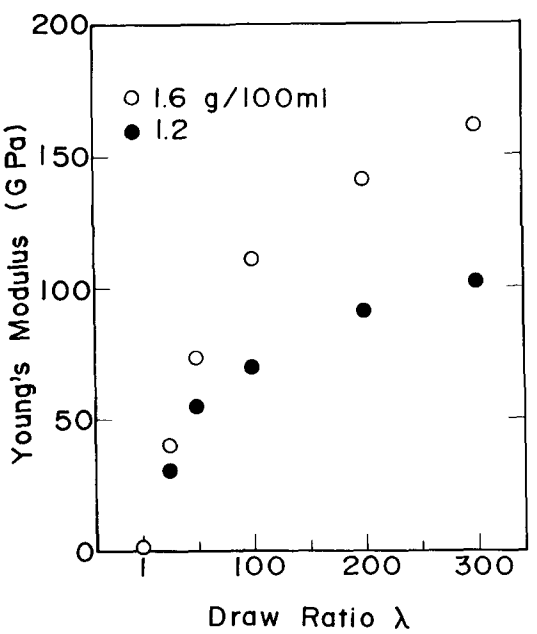

Figure 4 Young's modulus *versus* draw ratio measured for the gel films prepared from solutions with concentrations of 1.2 and 1.6 g/100 ml for polyethylene with $MW = 1 \times 10^6$

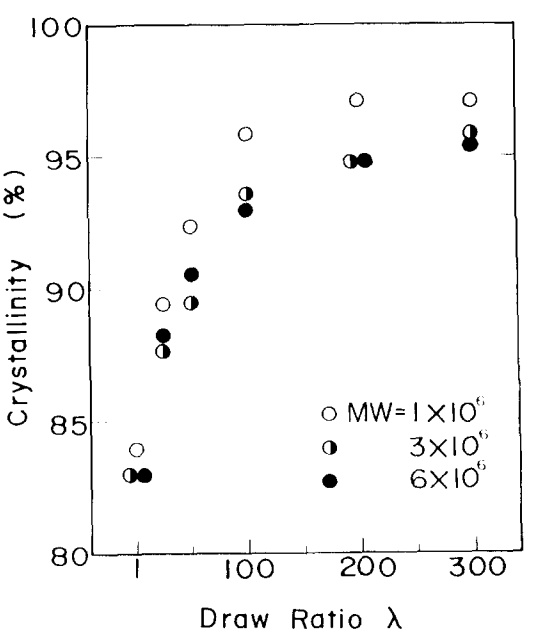

Figure 5 Crystallinity *versus* draw ratio for the dried gel films with the indicated molecular weights

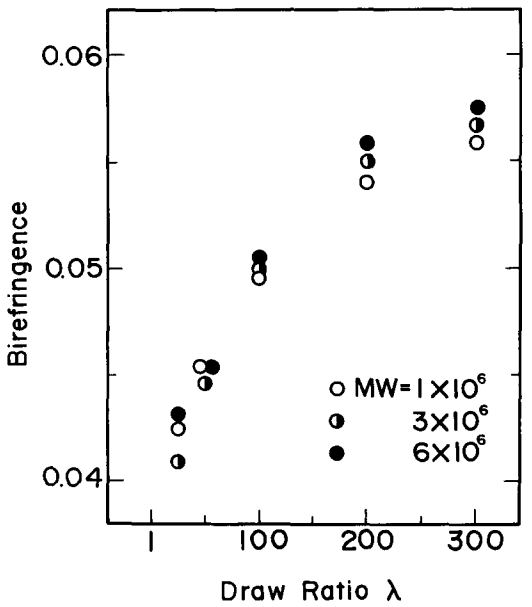

Figure 6 Birefringence *versus* draw ratio for the dried gel films with the indicated molecular weights

ratio λ for the three kinds of specimens. The values increase with increasing λ. The value for UHMWPE with $MW = 1 \times 10^6$ is highest among the three specimens at each draw ratio but the difference is only within 4%. At $\lambda = 300$, the values for all the specimens are beyond 95%.

Figure 6 shows the variation of birefringence with draw ratio λ. The birefringences for all the specimens showed a considerable increase up to $\lambda = 25$ and a gradual increase beyond $\lambda = 25$. Incidentally, macroscopic observations up to $\lambda = 25$ revealed that the drawing process is non-uniform and the decrease in the transverse dimension with increasing length due to elongation occurred mainly in the direction of the film thickness and much less in the film width. Such a necking deformation hampered the measurements of birefringence for specimens whose draw ratios are less than 25.

In order to obtain more detailed information for molecular orientation, the second-order orientation factors of three principal crystallographic axes are observed as a function of draw ratio λ. *Figure 7* shows the results, in which F^j_{20} characterizes the crystallite orientation distribution with variation between $-1/2$ and 1. For random orientation of the jth axis, F^j_{20} is 0, while for complete orientation parallel and perpendicular to the stretching direction, F^j_{20} is unity and $-1/2$, respectively. The orientation factors of the c axis were obtained by two methods: one is measured directly from the (0 0 2) plane and the other calculated from the orientation factors of the a and b axes using Wilchinsky's equation[9].

As can be seen in *Figure 7*, for all the specimens, the c axes obtained by both methods are oriented almost perfectly with respect to the stretching direction even at an initial draw ratio such as $\lambda = 25$, while the a and b axes are perpendicular to the stretching direction. The value of F^j_{20} for the a axes is almost equal to that for the b axes, indicating the random orientation of crystallites around the c axis. This indicates that the preferential orientation of the c axis is due to a significant crystal transformation from a folded to a fibrous type, but not due to a rotation of crystallites around their b axis, which is usually observed under the drawing process of polyethylene film with spherulitic textures[10]. Infra-red spectra in *Figure 8* support the above concept. With increasing λ, the *gauche* band becomes indistinct and disappeared entirely at $\lambda = 300$.

Figure 9 shows the change in the profiles of the d.s.c. curves at $\lambda = 50$ and 300 for three kinds of specimens. In all cases, the profile shows a single main peak in addition to a small shoulder. As can be seen in this figure, the peak position at $\lambda = 50$ and 300 approaches a constant value of around 154°C for specimens with $MW = 1 \times 10^6$ and 3×10^6, while for the specimen with $MW = 6 \times 10^6$ the peak position shifts slightly to higher temperature from 154 to 156°C. The higher melting temperature of the present specimens compared with the equilibrium melting point (145.5°C)[11] has been explained by assuming that the polymer chains in the melt retained the extended-chain arrangement and the entropy of fusion would obviously be smaller than the value calculated for the transformation from fully crystalline extended-chain polyethylene to random coils in the melt[12,13]. Judging from the profiles of d.s.c. curves, it turns out that the crystal size and crystallinity of the present specimens with each draw ratio are almost independent of molecular weight.

Table 3 presents the Young's moduli with draw ratio for the two kinds of specimens. These values were described in the range between minimum and maximum values, since the values were scattered. The Young's modulus increases with draw ratio. According to Hooke's law, the Young's modulus of solid polymer depends on the molecular orientation and must level off at $\lambda \geqslant 100$, since the orientation factor of the c axis of the specimens with $\lambda \geqslant 100$ is almost unity, as shown in *Figure 7*. This assumption contradicts the experimental results in *Table 3*. This assumption is probably due to the fact that Hooke's law applies to continuous mechanical theory. However, the concepts of this theory cannot be applied to crystalline polymer systems. As for the crystalline polymer systems, it would be expected that the Young's modulus is quite sensitive to the crystal size, the number of entanglements and/or tie molecules, the number of voids and the crystallinity in addition to the molecular orientation.

In order to obtain more conclusive evidence for the above concept, the stress relaxation modulus as a function of temperature was obtained for drawn films with three values of molecular weight. *Figures 10* and *11* show the temperature dependence of the stress relaxation modulus $Y(t)$ as a function of time for undrawn films ($\lambda = 1$) and drawn films with $\lambda = 300$. The measurements were carried out for the three molecular weights. It can be seen that all the stress relaxation moduli decrease with increasing temperature at a given time, as well as with increasing time at a fixed temperature. Closer observations reveal that the magnitude of $Y(t)$ of the undrawn films with increasing time shows a gradual decrease and this tendency is independent of the molecular weight. In contrast, the magnitude of $Y(t)$ of the drawn films ($\lambda = 300$) shows a considerable decrease with increasing time beyond 100 s in the temperature range 100–130°C. This tendency is enhanced for the specimen with $MW = 1 \times 10^6$. This is probably due to the fact that the number of entanglement meshes per molecule of the specimen with $MW = 1 \times 10^6$ is fewer than that within the specimen with $MW = 6 \times 10^6$, and partial slippage between molecular chains due to active molecular motion

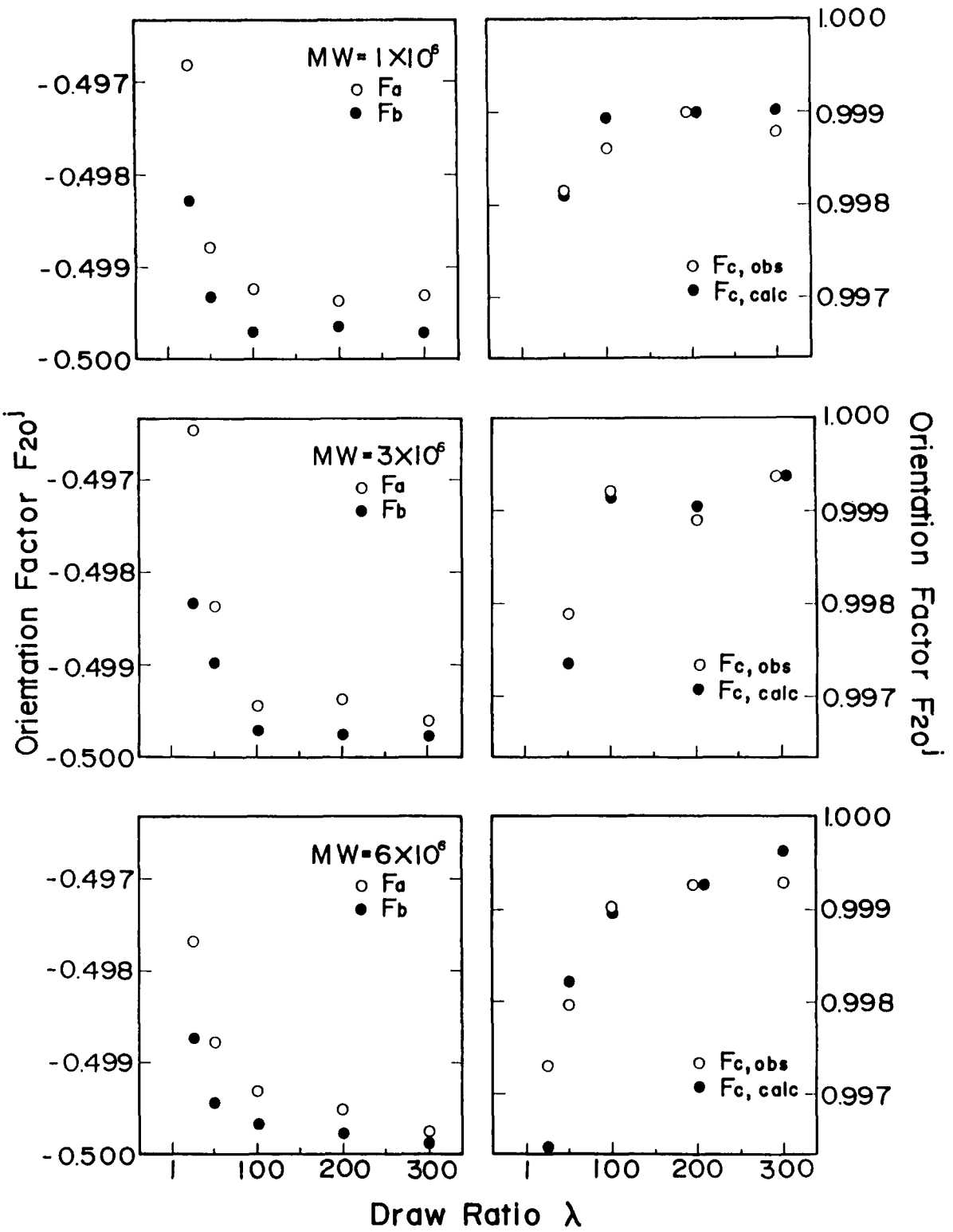

Figure 7 The second-order orientation factors of the *a*, *b* and *c* axes for the dried gel films with the indicated molecular weights. F_a, F_b and $F_{c,obs}$ are calculated from the orientation distribution functions of the (1 1 0), (2 0 0) and (0 0 2) planes and $F_{c,calc}$ is obtained from the second-order orientation factors of the *a* and *b* axes

Table 3 The Young's modulus (GPa) of two kinds of dried gel films at various draw ratios

Molecular weight, *MW*	Draw ratio, λ					
	1	50	100	200	300	400
1×10^6	1.8	42–94	63–149	99–177	124–201	–
3×10^6	1.7	51–98	118–154	134–196	148–210	142–205

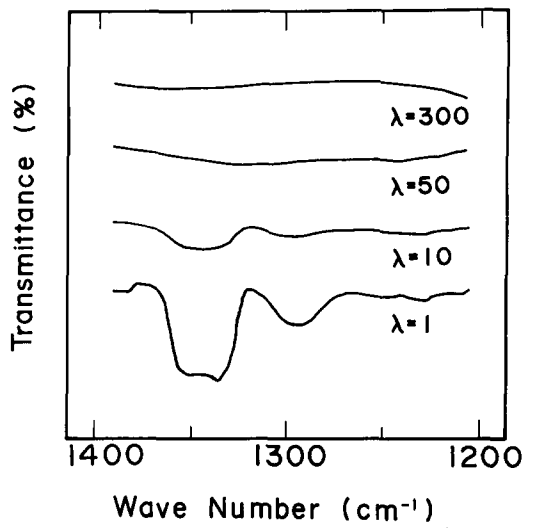

Figure 8 Infra-red spectra with increasing draw ratio for the dried gel films with $MW = 6 \times 10^6$

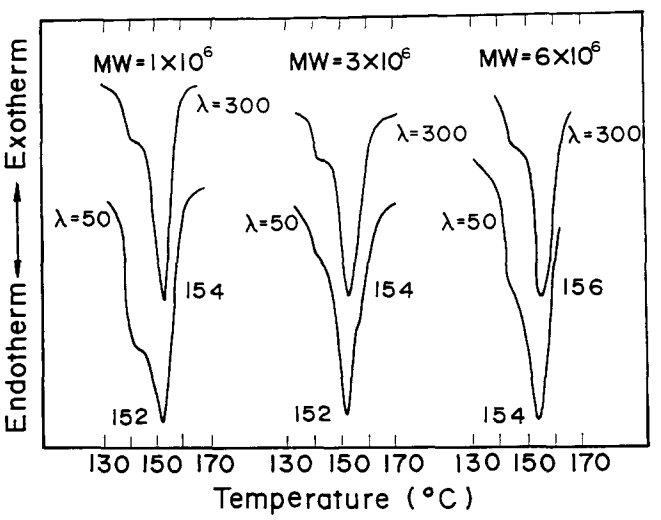

Figure 9 Profiles of the d.s.c. curves at $\lambda = 50$ and 300 for dried gel films with the indicated molecular weights

at $T > 100°C$ causes unlacing of the entanglement mesh and subsequently the decrease in the stress relaxation modulus.

Figures 12 and *13* show the master curves for the gel films with draw ratios of 1 and 300, reduced to the common reference temperature of 70°C. Each curve is obtained by shifting horizontally and then vertically until good superposition is achieved. It is seen that the master curves for undrawn films exhibit a linearly decreasing line, while the profiles of the master curves for the three kinds of drawn films depend on the master curves. Namely, the stress relaxation modulus of the drawn film with $MW = 1 \times 10^6$ exhibits a drastic increase in magnitude with increasing time but the other two curves show a gradual decrease. This phenomenon is of interest in considering the relationship between molecular weight and durability. The result in *Figure 13* indicates that, among the three ultradrawn polyethylenes, the specimen with $MW = 6 \times 10^6$ is the most advantageous as an industrial material because it exhibits the smallest decrease in stress relaxation modulus on long-term standing in the timescale $> 10^6$ s. This is probably due to the fact that the higher the molecular weight, the greater the number of entanglement meshes per molecule. Hence the unlacing of entanglement meshes within the specimen with $MW = 6 \times 10^6$ is slowest on decrease of the stress relaxation modulus among the specimens.

According to numerous studies[14–23], the α transition of polyethylene has been reported to consist of two or more relaxation mechanisms. From their observations, however, it can be inferred that the direct separation of the reduced modulus into the respective contributions cannot be carried out owing to the lack of adequate data, especially in the lower-frequency range and/or on the shorter timescale. In order to classify the broad dispersion curve into two or more components, the logarithm of the temperature dependence of the horizontal shift factor $a_T(T, T_0)$ has been plotted against reciprocal absolute temperature. For the same reason, Arrhenius plots were carried out in addition to those for specimens with $\lambda = 1$, 50 and 300 in this experiment. The plots on the left in *Figures14–16* show each result. The plots on the right in *Figures 14–16* show the temperature dependence of the

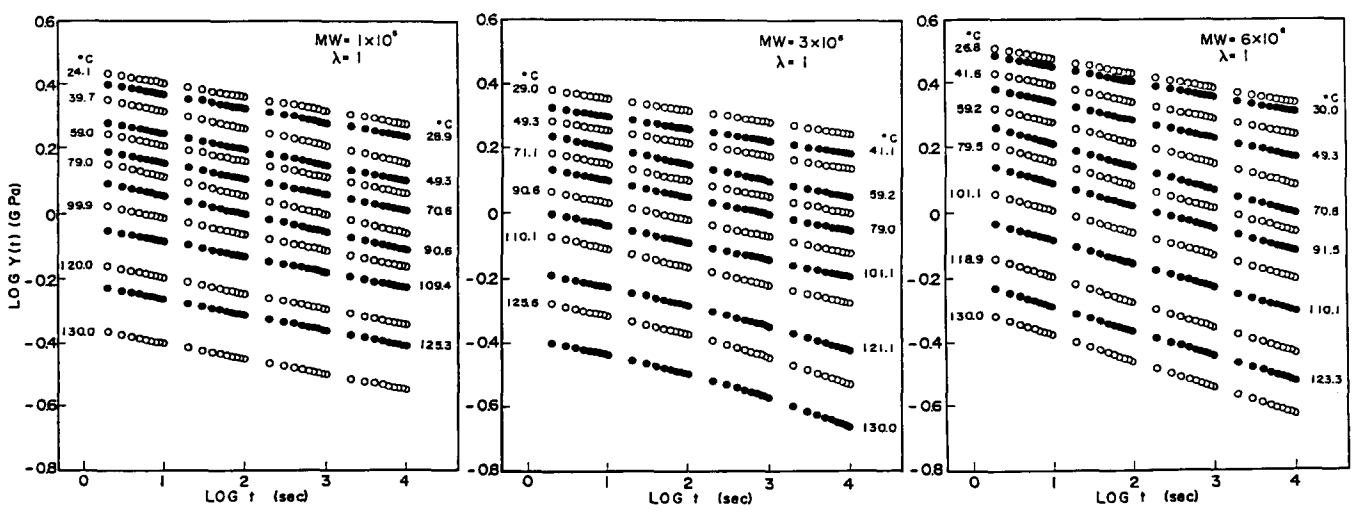

Figure 10 Temperature dependence of the stress relaxation modulus as a function of time for undrawn films ($\lambda = 1$) with the indicated molecular weights

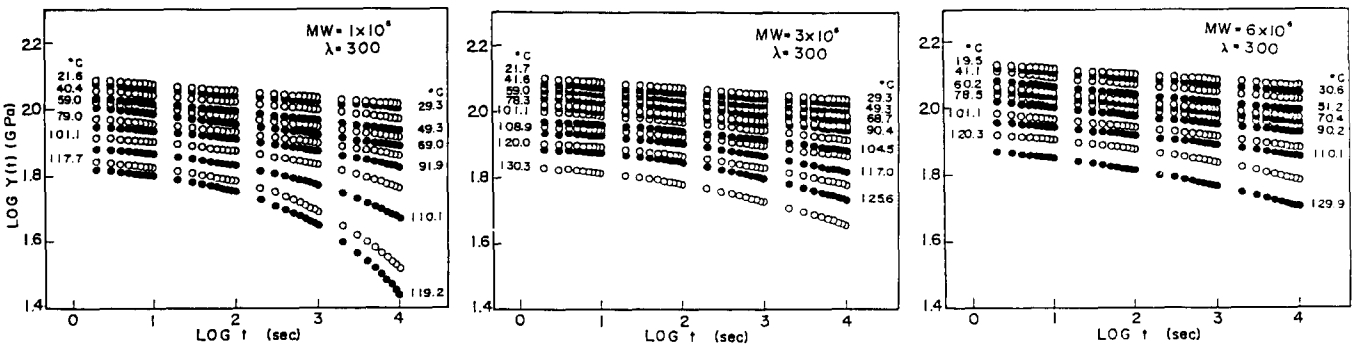

Figure 11 Temperature dependence of the stress relaxation modulus as a function of time for drawn films ($\lambda = 300$) with the indicated molecular weights

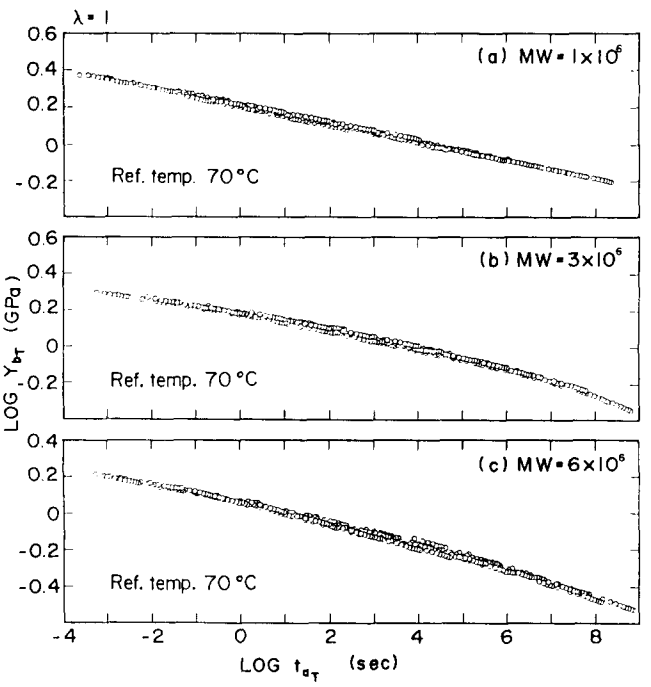

Figure 12 Master curves of the stress relaxation modulus for the undrawn films ($\lambda = 1$) with the indicated molecular weights

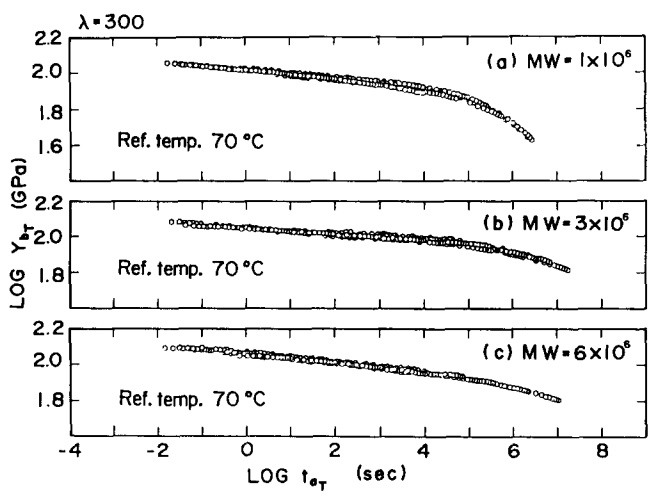

Figure 13 Master curves of the stress relaxation modulus for the drawn films ($\lambda = 300$) with the indicated molecular weights

vertical shift factor $b_T(T, T_0)$ of the stress relaxation modulus to realize the temperature–time superposition. The Arrhenius plots thus obtained are represented by two straight lines for the undrawn films and by three straight lines for the drawn films. For the undrawn films, two activation energies are obtained from the slopes of these lines. The low-temperature mechanism is in the range 162–163 kJ mol^{-1} and the high-temperature mechanism in the range 330–335 kJ mol^{-1}.

According to the measurements of complex dynamic tensile moduli by Takayanagi *et al.*[22,23], the temperature–frequency superposition of polyethylene single-crystal mats required only a horizontal shift along the logarithmic frequency axis, and the activation energy was evaluated as 192 kJ mol^{-1} associated with the α_2 mechanism. Thus, they concluded that such a simple superposition phenomenon for the α_2 mechanism is due to the dispersion associated with a single coefficient of internal friction, which uniquely determines the temperature dependence of the relaxation time associated with all of the vibrational modes. Furthermore, they pointed out that there exists no contribution of the α_1 mechanism for the crystal dispersion of the single-crystal mats.

Judging from the concept of Takayanagi, the low-temperature mechanism in *Figure 14* corresponds to the α_2 dispersion. The high-temperature mechanism is unknown, but this is probably due to a greater contribution to the stress relaxation modulus from mechanism III reported by Nakayasu *et al.*[14]. This is in accordance with the fact that the dispersions formed at high temperatures have greater apparent activation energies. According to the measurements of complex dynamic modulus in the previous paper[6], the loss modulus above 90°C exhibited unusual behaviour, in which the increase in the magnitude of the loss modulus with decreasing frequency becomes abruptly more pronounced in the range below 5 Hz, indicating the existence of mechanism III. These unusual trends pose problems in constructing master curves by frequency–temperature superposition. This tendency is quite different from the current results. Namely, using the stress relaxation method, the master curves can be constructed and subsequently the activation energies of mechanism III can be estimated as 330–335 kJ mol^{-1} from the Arrhenius plots, which has never been obtained by the dynamic measurements. The α_1 mechanism was not observed. This is similar to the behaviour of single-crystal mats reported by Takayanagi[22,23] but is quite different from the result for the

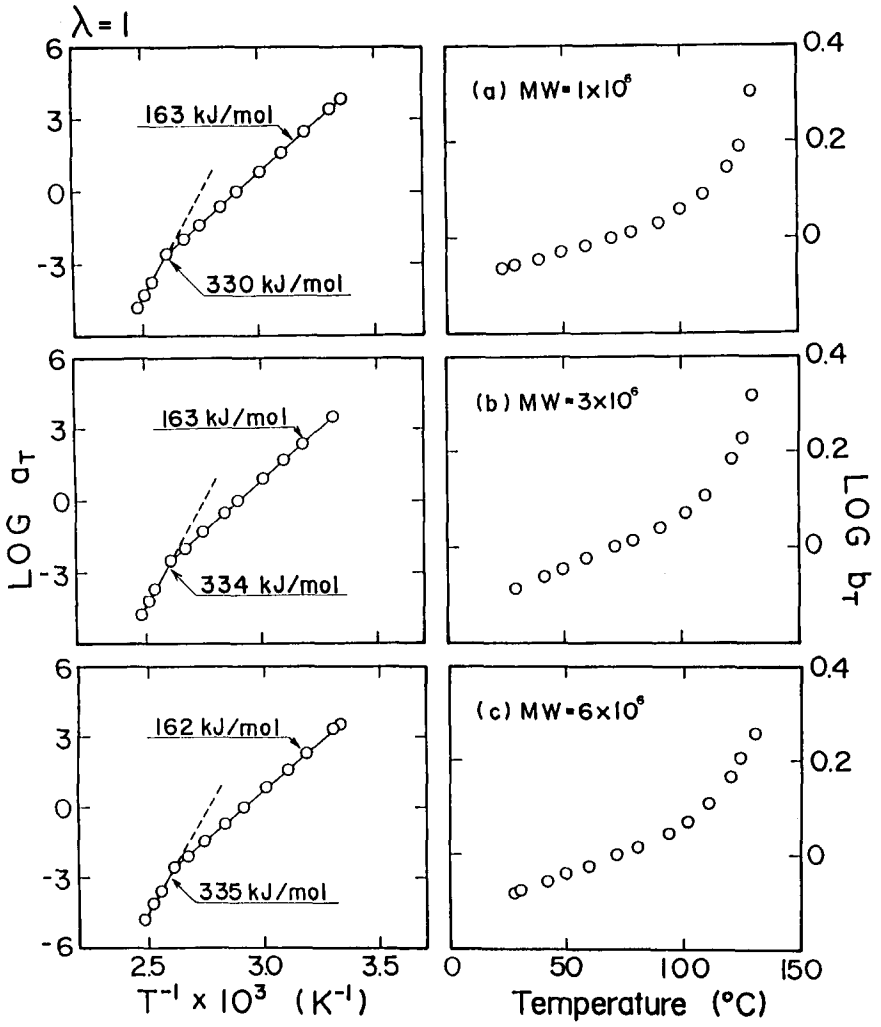

Figure 14 Arrhenius plots of the horizontal shift factors $a_T(T, T_0)$ and the logarithm of the vertical shift factors $b_T(T, T_0)$ *versus* temperature for the undrawn films ($\lambda = 1$) with the indicated molecular weights

gel film used in the previous work[6] for the measurements of complex dynamic modulus in spite of the same sample preparation method. A question can be raised as to whether the relaxation mechanism obtained from the stress relaxation modulus is equivalent to that obtained from dynamic measurement. If both relaxation mechanisms are the same, the difference indicates the difficulty in controlling the detailed morphology at the laboratory level. That is, the crystal lamellae with the previous gel films have a number of crystal defects and consequently are less ordered than those with the gel films in this experiment. If the α_1 mechanism is associated with inter-crystal-mosaic-block relaxation within the lamellae, as reported by Suehiro *et al.*[24–27], the imperfections of crystal lamellae cause the α_1 mechanism.

Here it should be noted that the activation energies associated with the α_2 and α_3 mechanisms are independent of molecular weight. This is probably attributed to a small dependence of molecular weight on crystallinity and long period as listed in *Table 2*. As can be seen, from the right side in *Figure 14*, the temperature dependence of $b_T(T, T_0)$ is pronounced with increasing temperature when plotted in logarithmic terms against a linear scale of temperature. It is noteworthy that, in the region of the α_2 mechanism, the superposition can be realized by a very small amount of vertical shift, while in the region of the α_3 mechanism, the vertical shift is significant in construction of the master curve. The behaviour of the α_2 mechanism is in good agreement with the results by Takayanagi *et al.*[22,23] reported for single-crystal mats.

The Arrhenius plots in *Figures 15* and *16* indicate that there exist three relaxation mechanisms, termed α_1, α_2 and α_3 mechanisms in order of increasing temperature. As indicated in these figures, the activation energies of the α_1 and α_2 mechanisms decrease with increasing draw ratio, but the relationship between draw ratio and activation energies for the α_3 mechanism is not clear.

Figure 17 shows the Arrhenius plots of the horizontal shift factor $a_T(T, T_0)$ and the logarithm of the vertical shift factor $b_T(T, T_0)$ *versus* temperature for the specimen drawn to $\lambda = 400$. The Arrhenius plots are represented as two straight lines. This result indicates that there exist two dispersions whose activation energies are 78 and 216 kJ mol^{-1}, respectively. The vertical shift is significant in construction of the master curves. According to Takayanagi[22,23], the temperature–frequency superposition associated with the α_2 mechanism required only a horizontal shift but the superposition associated with the α_1 mechanism can be realized by horizontal and vertical shifts. Therefore, the low- and high-temperature mechanisms can be denoted as α_1 and α_3, respectively. However, this analysis is different from the previous one already

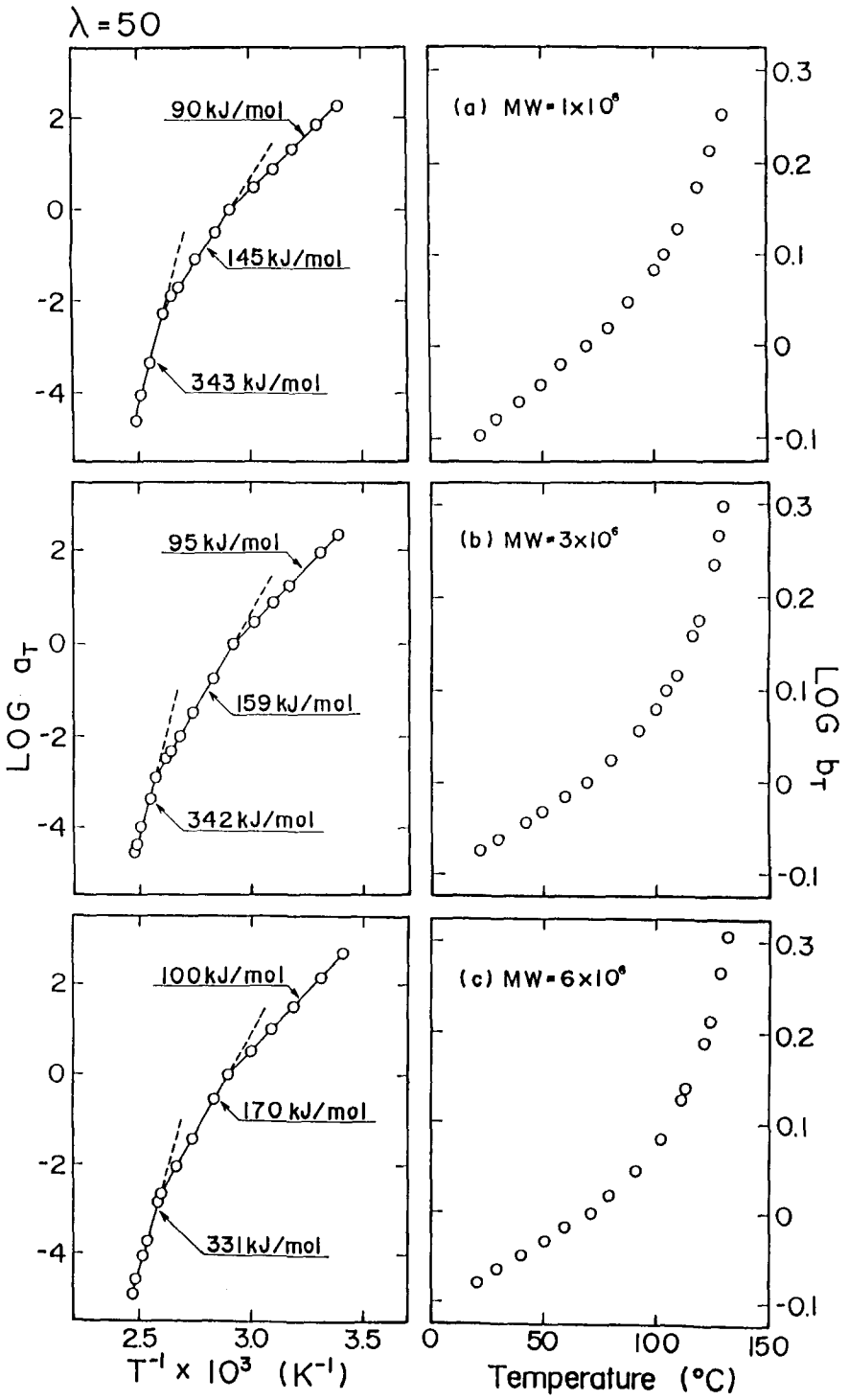

Figure 15 Arrhenius plots of the horizontal shift factors $a_T(T, T_0)$ and the logarithm of the vertical shift factors $b_T(T, T_0)$ *versus* temperature for the drawn films ($\lambda = 50$) with the indicated molecular weights

discussed elsewhere[6]. Namely, the Arrhenius plots were represented as a straight line from the superposition of loss modulus, in spite of using the same specimen. The superposition of the loss modulus required only a horizontal shift along the logarithmic frequency axis and that of the storage modulus required a very small vertical shift in addition to the horizontal one. A question, however, can be raised as to why the superposition process between stress relaxation and dynamic modulus measurements is different in spite of using the same test specimen. It may be expected that the superposition of the stress relaxation modulus is not equivalent to that of the complex dynamic modulus because of the lack of linearity due to sample elongation during the measurements at temperatures above 100°C.

In spite of the unnecessary vertical shift, the dispersion can be designated as the α_1 mechanism in terms of molecular orientation, based on the concept of Suehiro *et al.*, which was derived from rheo-optical studies[24–26]. To explain this, we refer to their concept. They pointed out that the α_2 mechanism depends upon the temperature dependence of the crystal modulus of crystallites in the horizontal direction within spherulites, and the contribution of the α_2 mechanism is significant when the c axes

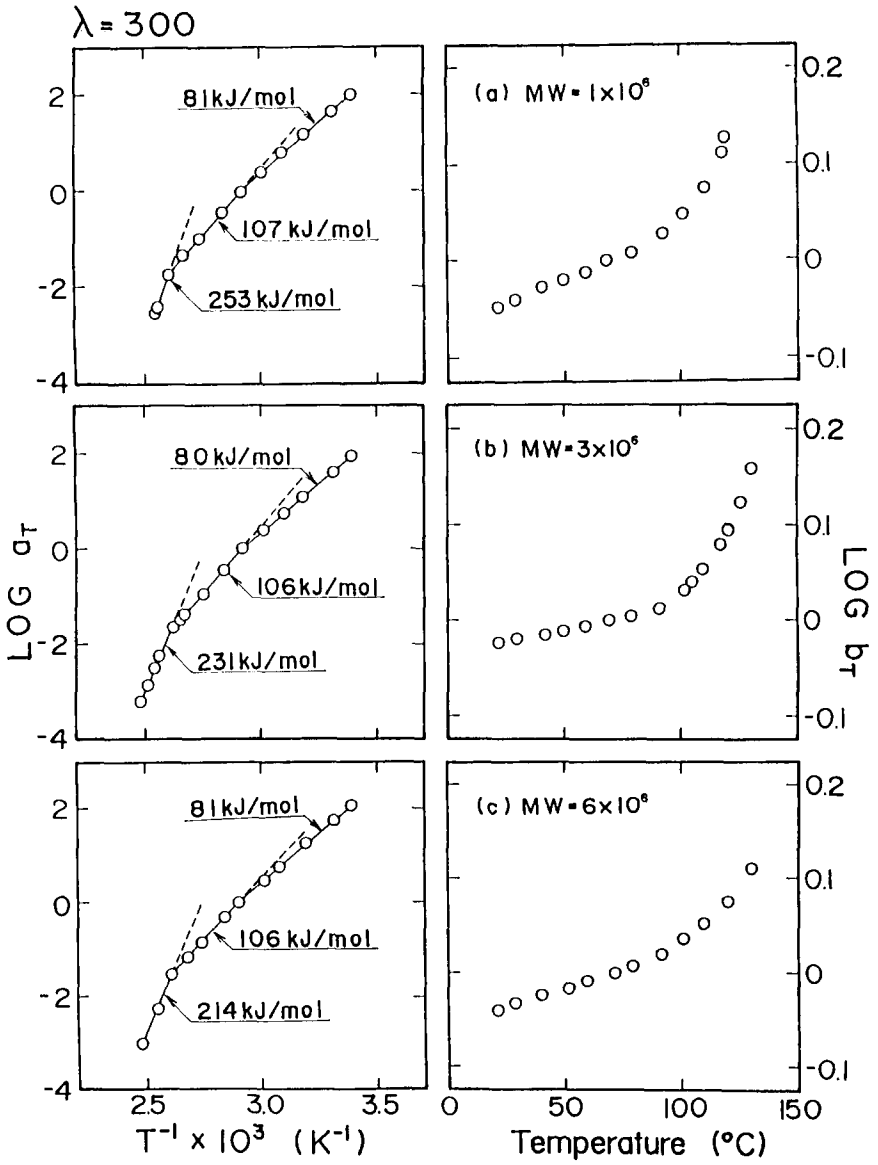

Figure 16 Arrhenius plots of the horizontal shift factors $a_T(T, T_0)$ and the logarithm of the vertical shift factors $b_T(T, T_0)$ *versus* temperature for the drawn films ($\lambda = 300$) with the indicated molecular weights

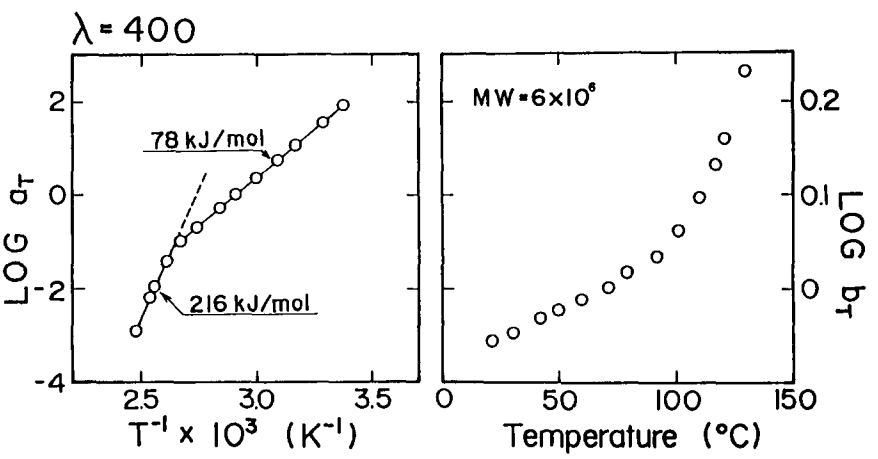

Figure 17 Arrhenius plots of the horizontal shift factors $a_T(T, T_0)$ and the logarithm of the vertical shift factors $b_T(T, T_0)$ *versus* temperature for the drawn films ($\lambda = 400$) with $MW = 6 \times 10^6$

Table 4 Activation energies of the α_1, α_2 and α_3 mechanisms of the dried gel films obtained as function of molecular weight and draw ratio

Molecular weight, MW	Draw ratio, λ	Activation energies (kJ mol^{-1}) α_1	α_2	α_3
1×10^6	1	–	163	330
	50	90	145	343
	300	81	107	253
3×10^6	1	–	163	334
	50	95	159	342
	300	80	106	231
6×10^6	1	–	162	335
	50	100	170	331
	300	81	106	214
	400	78	–	216

are oriented perpendicular to the external applied excitation. If this is the case, the α_2 mechanism does not appear for the ultradrawn film with $\lambda = 400$ because of almost perfect orientation of crystallites. Therefore, in the previous paper[6], the dispersion with an activation energy of 78 kJ mol^{-1} corresponded to the α_1 mechanism. It is evident that the above concept can be also constructed in the present paper.

Table 4 summarizes the change in activation energies of α_1, α_2 and α_3 mechanisms with draw ratio and molecular weight. Among the three mechanisms, the origin of the α_3 mechanism is not clear, and we shall use these results in referring to the α_1 and α_2 mechanisms. The dispersion strength of the α_2 mechanism becomes smaller with increasing λ and finally becomes zero at $\lambda = 400$. Therefore it was inferred that the α_2 mechanism is obviously observed when the external excitation is perpendicular to the c axis but is less obvious when the applied excitation is parallel to the c axis. Therefore if the α_2 mechanism is ascribed to the smearing-out effect of the crystal lattice potential due to onset of rotational oscillation of polymer chains within crystal grains, as pointed out by Kawai *et al.*[27], the smearing-out effect must be most active when the direction of the external applied stress is perpendicular to the c axis. This result supports the present conclusion that the α_2 mechanism is related to the anisotropy of crystallites.

The activation energy of the α_1 mechanism decreases with increasing draw ratio, indicating that the α_1 mechanism must be treated in relation to the relative orientation of molecular chains as in the case with the α_2 mechanism. The α_1 mechanism has been analysed from rheo-optical studies for polyethylene with spherulites[24–27]. If the α_1 mechanism for a spherulitic specimen is assigned to intralamellar grain boundary phenomena associated with reorientation of crystal grains due to their own preferential rotation within the orienting crystal lamellae, it may be expected that the α_1 mechanism of ultradrawn film is related to the slippage of crystal grains in the direction of the c axis. Namely, rotation of the crystallites cannot occur in an ultradrawn film when the external excitation is parallel to the stretching direction. If the value of the energy associated with the shear deformation parallel to the c axis is higher than that associated with the reorientation of crystal grains, the activation energy of the α_1 mechanism decreases with increasing draw ratio. This result also supports the result obtained by the dynamic measurement[6].

The activation energies associated with the α_1 and α_2 mechanisms are not sensitive to the molecular weight. As can be seen in *Table 2* and *Figures 5–7*, the morphological properties such as crystallinity and molecular orientation of undrawn and drawn films are hardly affected by the molecular weight. If the above concept of the α_1 and α_2 mechanism is justified, it is reasonable that both activation energies are almost independent of molecular weight.

CONCLUSIONS

The morphology and mechanical properties of polyethylene gel films have been studied using three kinds of specimens whose molecular weights are 1×10^6, 3×10^6 and 6×10^6. The morphological properties such as crystallinity and molecular orientation were not so sensitive to the molecular weights and have almost the same values for various draw ratios. The mechanical properties were mainly investigated in terms of crystal dispersion obtained by stress relaxation measurements. The temperature dependence of the stress relaxation modulus was measured in the range of time from 2 to 10^4 s. The master curves were constructed by shifting horizontally and then vertically. The stress relaxation modulus of drawn film with $MW = 1 \times 10^6$ exhibits a drastic decrease in magnitude with increasing time but the other two curves show a gradual decrease. The activation energies associated with the α_1 and α_2 mechanisms obtained by Arrhenius plots became lower with increasing draw ratio. This result is in good agreement with that obtained by the dynamic measurement. In contrast, the activation energies are almost independent of molecular weight. This result supports the concept that the morphological properties are correlated with activation energies associated with the α_1 and α_2 mechanisms.

REFERENCES

1 Smith, P., Lemstra, P. J., Kalb, B. and Pennings, A. J. *Polym. Bull.* 1979, **1**, 733
2 Smith, P. and Lemstra, P. J. *J. Mater. Sci.* 1980, **15**, 505
3 Smith, P., Lemstra, P. J. and Booij, H. C. *J. Polym. Sci., Polym. Phys. Edn.* 1981, **19**, 877
4 Smith, P., Lemstra, P. J., Pijpers, J. P. L. and Kiel, A. M. *Colloid Polym. Sci.* 1981, **259**, 1070
5 Sawatari, C., Okumura, T. and Matsuo, M. *Polym. J.* 1986, **18**, 741
6 Matsuo, M., Sawatari, C. and Ohhata, T. *Macromolecules* 1988, **21**, 1317
7 Matsuo, M. and Sawatari, C. *Macromolecules* 1986, **19**, 2036
8 Zapas, L. J. and Crissman, J. M. *Polymer* 1984, **25**, 57
9 Wilchinsky, Z. W. *J. Appl. Phys.* 1960, **31**, 1969
10 Matsuo, M., Hirota, K., Fujita, K. and Kawai, H. *Macromolecules* 1978, **11**, 1000
11 Flory, P. J. and Vrij, A. *J. Am. Chem. Soc.* 1963, **85**, 3548
12 Matsuo, M. and Manley, R. St J. *Macromolecules* 1983, **16**, 1500
13 Sawatari, C. and Matsuo, M. *Colloid Polym. Sci.* 1985, **263**, 783
14 Nakayasu, H., Markovitz, H. and Plazek, P. *J. Trans. Soc. Rheol.* 1961, **5**, 261
15 Takayanagi, M. and Matsuo, T. *J. Macromol. Sci. Phys. (B)* 1967, **1**, 407
16 Saito, N., Okano, K., Iwayanagi, S. and Hideshima, M. in 'Solid State Physics' (Eds. H. Ehrenreich, F. Seitz and D. Turnbull), Academic, New York, 1963, Vol. 14, p. 458
17 Tsuge, K., Enjoji, H., Terada, H., Ozawa, Y. and Wada, Y. *Japan. J. Appl. Phys.* 1962, **1**, 270
18 Iwayanagi, S. and Miura, I. *Japan. J. Appl. Phys.* 1965, **4**, 94
19 Tuijnman, C. A. F. *Polymer* 1963, **4**, 269
20 Tuijnman, C. A. F. *Polymer* 1963, **4**, 315

21 Stachurski, Z. H. and Ward, I. M. *J. Macromol. Sci. Phys.* (*B*) 1969, **3**, 445
22 Manabe, S., Sakado, A., Katada, A. and Takayanagi, M. *J. Macromol. Sci. Phys.* (*B*) 1970, **4**, 161
23 Kajiyama, T., Okada, T., Sakoda, A. and Takayanagi, M. *J. Macromol. Sci. Phys.* (*B*) 1973, **7**, 583
24 Suehiro, S., Yamada, T., Inagaki, H., Kyu, T., Nomura, S. and Kawai, H. *J. Polym. Sci., Polym. Phys. Edn.* 1979, **17**, 763
25 Suehiro, S., Yamada, T., Kyu, T., Fujita, K., Hashimoto, T. and Kawai, H. *Polym. Eng. Sci.* 1979, **19**, 929
26 Suehiro, S., Kyu, T., Fujita, K. and Kawai, H. *Polym. J.* 1979, **11**, 331
27 Kawai, H., Suehiro, S., Kyu, T. and Shimomura, A. *Polym. Eng. Rev.* 1983, **3**, 109